ELSEVIER

Journal of Power Sources 86 (2000) 469–477

JOURNAL OF POWER SOURCES

www.elsevier.com/locate/jpowsour

Process engineering of the direct methanol fuel cell

H. Dohle *, J. Divisek, R. Jung

Institut für Werkstoffe und Verfahren der Energietechnik, Forschungszentrum Jülich, 52425 Jülich, Germany

Accepted 26 October 1999

Abstract

A direct methanol fuel cell (DMFC) model has been developed and experimentally verified, with which fundamental calculations of the DMFC were carried out. Modelling comprises the mass transport of the gases in the diffusion layers and catalyst layers, mass transport in the membrane, as well as the reaction and the potential distribution in the catalyst layers. The performance of the fuel cell is adversely influenced by methanol permeation from the anode to the cathode. Moreover, the formation of a mixed potential is possible both at the anode and cathode and has a large negative effect on the energetic performance of the fuel cell. The model provides information concerning the impact of methanol permeation through the membrane on energy and mass yield, and on the influence of the operating and structural parameters.

Keywords: DMFC; Fuel cell; Modelling; Mixed potential

1. Introduction

Among the different fuel cell technologies, the direct methanol fuel cell (DMFC) with methanol as the energy carrier, has one of the highest application prospects as an energy converter for environmentally benign vehicles. The DMFC, which is a further development of familiar hydrogen polymer electrolyte membrane (PEM) technology, presently still has to overcome problems with respect to efficiency and power density. Even if the thermodynamic reversible potentials for both methanol/oxygen and hydrogen/oxygen cells are largely equivalent and have comparable values (1.21 vs. 1.23 V), the cell output voltage is very different. The hydrogen fuel cell has a much higher cell voltage and the main losses are essentially associated with poor electrocatalysis at the oxygen electrode. In addition to this difficulty, which is the same for both cell types, the DMFC cell has a number of further serious process engineering problems which, on one hand, are associated with methanol permeation through the polymer membrane and, on the other hand, with sluggish catalysis of the electrochemical methanol oxidation. Methanol permeation through the polymer membrane reduces the mass yield and, moreover, is responsible for mixed potential formation at the cathode, which further reduces the energy yield of the cell.

In a DMFC, the following catalytically activated reactions, which are spatially separated from each other, take place:

$$\text{anode: } CH_3OH + H_2O \Rightarrow CO_2 + 6H^+ + 6e^- \quad (1)$$

$$\text{cathode: } 6H^+ + 6e^- + 1.5O_2 \Rightarrow 3H_2O. \quad (2)$$

One of the main problems of the DMFC is the multistage nature of the anodic reaction (1). In DMFCs, CO or COH occurs as a stable, adsorbed intermediate of methanol oxidation. Poisoning of the anode catalysts by these adsorbates leads to considerable anodic overpotentials compared to the theoretically possible cell voltages. At anode potentials below about +500 mV vs. the reversible hydrogen potential, the oxidation of methanol is initiated by a dehydrogenation reaction of the methanol [1]. At higher potentials, methanol oxidation probably takes place through a reaction with adsorbed oxygen or OH [2].

The basic scheme of a DMFC fuel cell is shown in Fig. 1. The methanol/water reaction mixture diffuses through the porous anode to the electrochemically active reaction zone in the immediate vicinity of the membrane, where the electrochemical oxidation of the methanol takes place. The CO_2 reaction product diffuses back into the anode channels. The protons formed entrain certain amounts of water

* Corresponding author.

0378-7753/00/$ - see front matter
PII: S0378-7753(99)00456-5

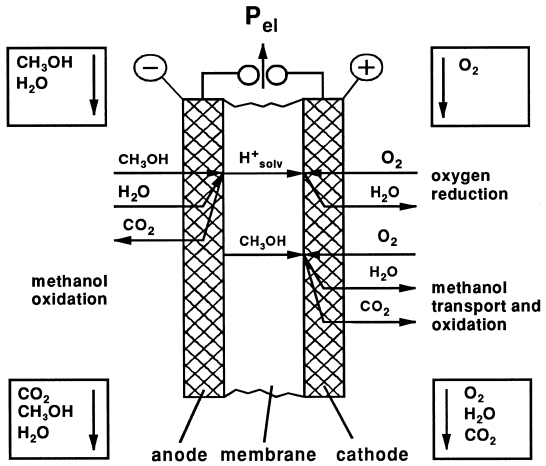

Fig. 1. Schematic diagram of the DMFC single cell with solid polymer electrolyte.

into the solvating envelope and, under the influence of the electric field, migrate [1] to the cathode where they react with oxygen to form water after electron acceptance. In addition, an undesired methanol transport from the anode to the cathode takes place caused by diffusion and electro-osmotic effects. The methanol fractions arriving at the cathode react with the oxygen present there to form CO_2.

Due to their high chemical stability, perfluorinated sulphonated cation exchangers are chiefly used at present as the membrane electrolyte. NAFION® from DuPont has played a central role in the development of polymer electrolyte fuel cells.

2. Experimental facilities and MEA preparation

The DMFC test rig consists of a cell with anodic and cathodic peripheries. The aqueous methanol solution circulates in the anode loop from which the cell is supplied with methanol. Spent methanol is continuously replaced and the CO_2 formed is removed. On the cathode side, oxygen or air is fed to the cell. The cell is kept at a constant temperature during test operations. The test cell used for the membrane electrode assembly (MEA) was a titanium cell with an active electrode area of 20 cm^2. Electronic contact with the MEA and the supply of reaction media was accomplished via a plate provided with separate feet (Fig. 2). The cell plates were fabricated from the solid metal.

The cell had lateral channels drilled for the supply and extraction of the reactants, for the current probe and for voltage measurement. The electrode potentials were measured vs. the hydrogen electrode (RHE).

The MEAs investigated were prepared as follows. The anode consisted of a carbon cloth support onto which a layer of uncatalysed XC-72 active carbon in an amount of 8 mg/cm^2 bonded with 5% PTFE was deposited. The catalytic layer contained 4 mg/cm^2 of Pt/Ru catalyst (50:50) on carbon and 20% NAFION from a 5% solution with water and low aliphatic alcohols. The cathode was similarly constructed with 4 mg/cm^2 of Pt catalyst on carbon bonded with 30% PTFE and an identical uncatalysed layer which served as the backing layer. The MEA was fabricated by hot pressing the two electrodes together with the NAFION 117 membrane in between them.

3. Mathematical model and model parameters

The model structure of the DMFC investigated is shown in Fig. 3a. It consists of a channel system incorporated into the structure of the electrode plate and an electronic conductor system formed by the feet. The diffusion region of the electrode (backing layer) is located adjacent to the electrode plate and consists of a highly porous electronic conductor based on catalytically inactive carbon. The other layer of the MEA facing the electrolyte membrane is the catalyst layer consisting of a catalyst carbon/NAFION electrolyte mixture. The PEM is located in the middle.

The arrangement shown in Fig. 3a is divided into seven regions (Fig. 3b) by means of a model division of the DMFC which represent the basic structure of the cell: the anodic and cathodic gas diffusers supplied with fuel gas or oxidant through the respective channels, the anodic and cathodic catalyst layers and the polymeric ion conductor in the middle of the cell. The gas components under consideration are methanol, steam, oxygen, carbon dioxide and nitrogen.

The model is one-dimensional, steady-state and isothermal. The one dimensional calculation leads to an error of approx. 8% in comparison to two dimensional calculations [3]. This relatively small error is caused by the specific combination of diffusion coefficients, conductivities of electronic and ionic phases, electrochemical charge transfer coefficients as well as electrode porosity.

The model calculations take account of mass transport in the gas diffuses, in the catalyst layers and in the membrane. In addition, the electrochemical concentration-dependent reactions take place in the catalyst layers. Mass transport within the electrolyte is in part diffusive and in part caused by electroosmosis. Apart from the membrane, there is also an ion-conducting electrolyte within the catalyst layers [4]. The numerical calculation is based on the finite integration technique (FIT) and was performed on the mathematical and physicochemical basis of an earlier-

[1] Ed. note: according to classical, hard-sphere interpretations. See alternative quantum tunneling models.

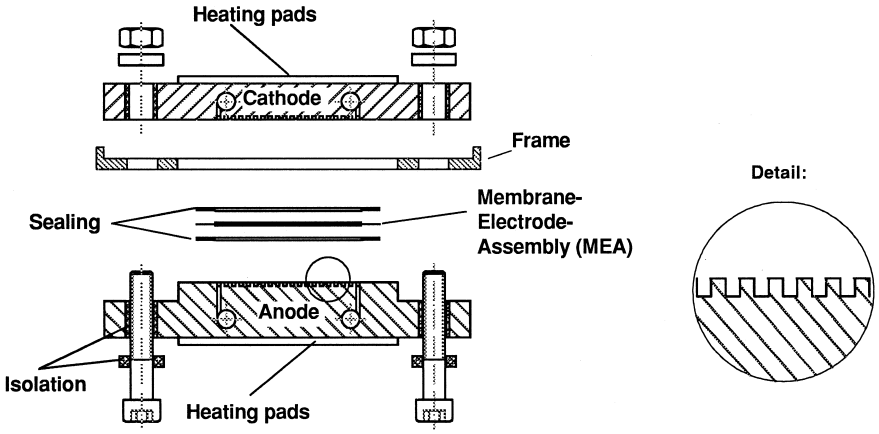

Fig. 2. Schematic diagram of the experimental small-scale DMFC.

developed H_2-PEM fuel cell model [5]. The individual model assumptions will be described in the following.

3.1. Channels

The reactants flow into the channels adjacent to the catalyst layers with a defined molar flow, $N_{i,\text{in}}$. The outlet molar flows, $N_{i,\text{out}}$, can first be determined by balancing the incoming molar flows, $N_{i,\text{in}}$, and the molar flows $N_{i,\text{edge}}$ flowing over the edges to the catalyst layers.

$$N_{i,\text{in}} = N_{i,\text{out}} + N_{i,\text{edge}}. \quad (3)$$

The composition of the gas mixture with the mole fractions y_i in the channels will be the same as in the channel outlet flow due to the intimate mixture being assumed as ideal.

$$y_i = \frac{N_{i,\text{out}}}{\sum N_{i,\text{out}}} \text{ with } N_{i,\text{out}}$$

= mass flow of the ith gas from the channel. (4)

By connecting the one-dimensional elements shown in Fig. 4 in series, it is possible to calculate the formation of a concentration profile as a function of the volume flow.

3.2. Gas diffuser

The pore radius in the gas diffusers is of the order of 100–1000 nm. This is a transition region for which several

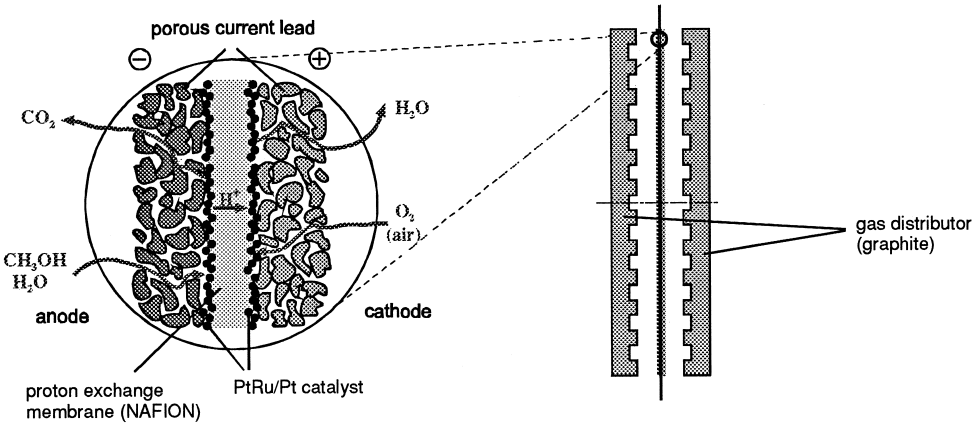

channel anode	diffusion layer	catalyst layer	membrane	catalyst layer	diffusion layer	channel cathode
- ideal intimate mixture	- diffusion - permeation in the gas phase	- diffusion - electroosmosis - reaction	- diffusion - electroosmosis	- diffusion - electroosmosis - reaction	- diffusion - permeation in the gas phase	- ideal intimate mixture
I	II	III	IV	V	VI	VII

Fig. 3. (a) Model of the DMFC structure. (b) Division of the cell into functional regions.

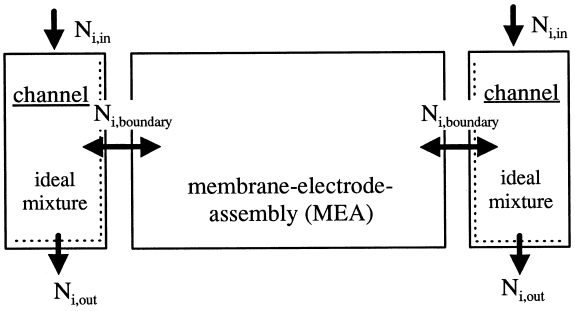

Fig. 4. Assumptions for the intimate mixture at the gas channel/electrolyte phase boundaries.

mass transport modes must be taken into account according to the mean transport pore model (MTPM) [6,7]. The molar flux, N_i, inside the gas diffusers can thus be expressed by a superposition of Stefan–Maxwell diffusion, Knudsen diffusion and Darcy permeation. Mass transport according to the MTPM, takes place in cylindrical capillaries with a mean radius of $\langle r \rangle$. Another characteristic parameter of the MTPM theory is the mean value of the pore radius squared, $\langle r^2 \rangle$, which enters into the calculation for the transport coefficients, B_i, for the permeation fraction. The derivation is contained in Appendix A.

The diffusion takes place in the transition region by a superposition of Knudsen diffusion and Stefan–Maxwell diffusion:

$$\frac{N_i^{\mathrm{d}}}{D_i^{\mathrm{k}}} + \sum_{j=1}^{n} \frac{y_j N_i^{\mathrm{d}} - y_i N_j^{\mathrm{d}}}{D_{i,j}^{\mathrm{m}}} = -c_{\mathrm{tot}} \frac{\mathrm{d}\, y_i}{\mathrm{d}\, x}. \tag{5}$$

The molar flows due to a total pressure gradient are taken into consideration by the Darcy expression:

$$N_i^{\mathrm{p}} = -y_i B_i \frac{\mathrm{d}\, c_{\mathrm{tot}}}{\mathrm{d}\, x} \tag{6}$$

with:

$$B_i = D_i^{\mathrm{k}} + \frac{\langle r^2 \rangle \zeta p}{8\eta}. \tag{7}$$

The molar flows due to a total pressure gradient are taken into consideration by the Darcy expression:

$$N_i = N_i^{\mathrm{d}} + N_i^{\mathrm{p}}. \tag{8}$$

The mass transport can be expressed according to the MTPM [5,6] in a matrix notation by combining the transport fractions:

$$\mathbf{F}\underline{N} = -\frac{\mathrm{d}\underline{c}}{\mathrm{d}\, x} \text{ or } \underline{N} = -\mathbf{G}\frac{\mathrm{d}\underline{c}}{\mathrm{d}\, x}. \tag{9}$$

The formulation of this transport matrix is to be found in Appendix B.

The mass transport in the gas diffusers is source- and sink-free. Hence:

$$\mathrm{div}\, N_i = 0 \tag{10}$$

The electronic current produced or consumed in the catalyst layers flows through the gas diffusers towards the channel structure. This electronic current leads to a voltage drop via Ohm's law according to:

$$i_{\mathrm{el}} = \sigma_{\mathrm{el}}^{\mathrm{eff}} \nabla \varphi_{\mathrm{el}}. \tag{11}$$

3.3. Catalyst layer

The catalyst layer is modelled as a porous body which is filled with ionically conducting membrane material. Knudsen diffusion prevails due to the small pore radii. The local reaction rate can be described as a function of the local overpotentials and local concentrations. The expression for the cathodic reaction reads:

$$i_{\mathrm{c}} = i_{\mathrm{O,ref}}^{\mathrm{c}} \frac{p_{\mathrm{O_2}}}{p_{\mathrm{O_2 ref}}} \exp\left[-\frac{\alpha_{\mathrm{c}} F}{RT} (\varphi_{\mathrm{el}} - \varphi_{\mathrm{ion}} - \varphi_{\mathrm{O,ref}}^{\mathrm{c}} \right] \tag{12a}$$

where $p_{\mathrm{O_2,ref}}$ is a reference pressure, $i_{\mathrm{O,ref}}$ a reference exchange current, α_{k} the cathodic charge transfer coefficient, R the general gas constant and T the temperature [8,9].

The anodic reaction similarly reads:

$$i_{\mathrm{a}} = i_{\mathrm{O,ref}}^{\mathrm{a}} \frac{p_{\mathrm{MeOH}}}{p_{\mathrm{MeOH,ref}}} \frac{p_{\mathrm{H_2O}}}{p_{\mathrm{H_2O,ref}}} \times \exp\left[+\frac{\alpha_{\mathrm{a}} F}{RT} (\varphi_{\mathrm{el}} - \varphi_{\mathrm{ion}} - \varphi_{\mathrm{O,ref}}^{\mathrm{a}} \right]. \tag{12b}$$

These two partial reactions occur both at the anode and at the cathode, forming mixed potentials due to methanol passing from the anode to the cathode, and oxygen diffusing from the cathode to the anode. Introducing a local electrochemically produced current density i_{EC}, the conservation equations for the ionic and electronic potentials, thus, yields the following:

$$\sigma_{\mathrm{el}} \nabla^2 \varphi_{\mathrm{el}} = -\sigma_{\mathrm{ion}} \nabla^2 \varphi_{\mathrm{ion}} = (i_{\mathrm{a}} + i_{\mathrm{c}}) S_{\mathrm{cat}} = i_{\mathrm{EC}} S_{\mathrm{cat}} \tag{13}$$

where the value S_{cat} is the inner catalytic surface of the electrode.

The source–sink terms of the respective material are linked via Faraday's law to the respective local current density, so that, e.g., for methanol:

$$\mathrm{QS}_{\mathrm{Methanol}} = -\frac{i_{\mathrm{a}}}{6F}. \tag{14}$$

Analogous treatment of the other materials leads to complete coupling of the ionic and electronic potentials with the conservation equations for the mass flows.

Mass transport in the catalyst layers is considered as a parallel superposition of Knudsen diffusion and diffusion in the membrane phase. Using a factor ε as the fraction of the membrane phase in the catalyst layers results in the

following formulation for the determination of the diffusion coefficients in the membrane phase:

$$D_{\mathrm{mem},i}^{\mathrm{eff}} = \varepsilon_{\mathrm{mem}} D_{\mathrm{mem},i}. \quad (15)$$

3.4. Membrane electrolyte

The physical properties of the membrane are included in this model as follows:

– The ionic conductivity is dependent on the water content.
– The diffusion and the electro-osmotic drag of methanol and water are also dependent on the water content.

The water content ψ of the membrane is defined as the ratio of the number of water molecules to the number of SO_3^- groups per volume unit:

$$\psi = \frac{\text{number of water molecules/volume unit}}{\text{number of } SO_3^- \text{ groups/volume unit}}. \quad (16)$$

The water transport in the membrane is composed of two fractions: the osmotic drag and the diffusion due to gradients in the water content, ψ. An essential aspect is the dependence on the water content, which can be expressed as follows according to [10]:

$$N_{\mathrm{H_2O,diff}} = -D_{\psi}^{\mathrm{mem}} \frac{\mathrm{d}\psi}{\mathrm{d}x} \text{ with } D_{\psi}^{\mathrm{mem}} = \frac{\rho_{\mathrm{dry}}}{M_{\mathrm{M}}} D_{\psi}. \quad (17)$$

The diffusion coefficient depends on the water content ψ and the temperature T:

$$D_{\psi>4} = 10^{-6} \exp\left[2416\left(\frac{1}{303} - \frac{1}{273+T}\right)\right](2.563 - 0.33\psi + 0.0264\psi^2 - 0.00067\psi^3)\ [\mathrm{cm^2/s}]. \quad (18)$$

The water content of the membrane is a function of the relative humidity $a = p_{\mathrm{H_2O}}/p_{\mathrm{H_2O,sat}}$:

$$\psi = 0.043 + 17.81a - 39.85a^2 + 36.0a^3 \text{ for } 0 < a < 1. \quad (19)$$

$\psi = 14$ is valid for Nafion in equilibrium with saturated steam and ψ assumes the value of 22 in liquid water [11].

The conductivity σ of the membrane is a function of temperature and water content:

$$\sigma(T,\psi) = \exp\left[1268\left(\frac{1}{303} - \frac{1}{273+T}\right)\right] \times (0.005139\psi - 0.00326) \text{ for } \psi > 1. \quad (20)$$

The apparent electrophoretic drag on water molecules is assumed to be proportional to the ionic current and proportional to the water content [10]:

$$N_{\mathrm{H_2O,drag}} = n_{\mathrm{drag}}^{\mathrm{H_2O}} \frac{I_{\mathrm{ion}}}{F} \frac{\psi}{22} \ [T = 30^{\circ}\mathrm{C}] \text{ with } n_{\mathrm{drag}}^{\mathrm{H_2O}} = 2.5. \quad (21)$$

For liquid-operated DMFCs, drag coefficients ranging from 2 at 20°C up to 5 at a temperature of 130°C have been measured [11]. Methanol transport in the membrane is also composed of diffusion and protonic drag.

Methanol transport is treated similarly to water transport. In the literature, diffusion coefficients for methanol are specified for completely swollen membranes [12]. Since no measurements of the diffusion coefficient for methanol in membranes of different humidity are reported in the literature, a linear formulation is assumed with respect to the methanol content of the membrane.

In analogy to the water content, a relation between the methanol partial pressure of the gas phase and the methanol content of the membrane can be formulated. The methanol content $\gamma = \mathrm{MeOH}/\mathrm{H}^+$ can be regarded as a function of the methanol concentration.

This gives, analogous to Eq. (21):

$$\gamma = 14\delta \frac{p_{\mathrm{MeOH}}}{p_{\mathrm{MeOH,sat}}} \text{ with } \delta = \frac{n_{\mathrm{drag}}^{\mathrm{MeOH}}}{n_{\mathrm{drag}}^{\mathrm{H_2O}}} = 0.6 \text{ (linearized)} \quad (22)$$

where a drag factor of 2.5 is assumed for water and a drag factor of 1.5 for methanol.

The diffusion coefficient of methanol in the membrane, $D_{\gamma}^{\mathrm{mem}}$, is set proportional to the diffusion coefficient of water in the membrane, D_{ψ}^{mem}, as:

$$D_{\gamma}^{\mathrm{mem}} = kD_{\psi}^{\mathrm{mem}} \text{ with } k = 1. \quad (23)$$

Methanol diffusion is obtained with reference to Eq. (17) as:

$$N_{\mathrm{MeOH,diff}} = -D_{\gamma}^{\mathrm{mem}} \frac{\mathrm{d}\gamma}{\mathrm{d}x}. \quad (24)$$

The methanol drag is assumed to be linearly dependent on the methanol concentration relative to the saturation concentration of methanol:

$$N_{\mathrm{MeOH,drag}} = n_{\mathrm{drag}}^{\mathrm{MeOH}} \frac{I_{\mathrm{ion}}}{F} \frac{p_{\mathrm{MeOH}}}{p_{\mathrm{MeOH,sat}}} \text{ with } n_{\mathrm{drag}}^{\mathrm{MeOH}} = 1.5. \quad (25)$$

For the other gas components (CO_2, O_2, N_2) pure diffusion is assumed inside the membrane for reasons of simplicity. The mass transport in the membrane is source- and sink-free.

3.5. Transitions between model regions

At the boundary between the catalyst layers and the gas diffusers, current only flows through the electronically conducting phase. The existence of ionic current is spatially limited to the catalyst layer and the membrane. The

following is valid for the derivation of the ionic current at the boundaries to the gas diffusers:

$$\frac{\partial \varphi_{\text{ion}}}{\partial x} = 0. \tag{26a}$$

Analogously, an electronic current only flows in the catalyst layers and gas diffusers; no current flow through the membrane takes place. As in Eq. (26a), the following boundary condition for the electronic current thus applies at the phase boundaries between membrane and catalyst layers:

$$\frac{\partial \varphi_{\text{el}}}{\partial x} = 0 \tag{26b}$$

The respective partial pressure of a material in the gas phase corresponds to a saturation concentration in the membrane phase. For methanol and water, this relation is defined via Eqs. (19) and (22) in which the material content in the membrane phase is correlated via the relative humidity of the gas phase. For the other gases (oxygen, nitrogen, carbon dioxide), the interdependence of the respective partial pressure p_i and the concentration $c_{\text{mem},i}$ in the membrane phase via Henry's constants is valid:

$$c_{\text{mem},i} = \frac{p_i}{K_{\text{H},i}}. \tag{27}$$

The program for solving these expressions is based on the discretization of the above mass transport and reaction equations. For each point, the conservation equations for mass transport, ionic and electronic current flow, as well as ionic and electronic potentials, are valid. Balancing over all the points of the discretized model regions leads to a system of equations of the following form for each model parameter M under consideration:

$$\mathbf{A}\,M = \text{constant}. \tag{28}$$

The coefficient matrix **A** contains the coupling of each point with the adjacent volume elements of the discretized model region.

4. Results and discussion

The main goal of modelling is the understanding and correct interpretation of the phenomena occurring in the DMFC. This will be illustrated by a few examples.

One of the greatest problems of the DMFC is methanol permeation. An illustration of the methanol permeation rate through the cell is given in Fig. 5a. The permeation rate as a mass flow is converted into current density according to Faraday's law. The methanol transport through the cell is a function of the methanol concentration in the anode loop and of the current density. As expected, the methanol transport increases with increasing methanol concentration. At low concentrations, the permeation rate decreases with increasing current density due to the elevated

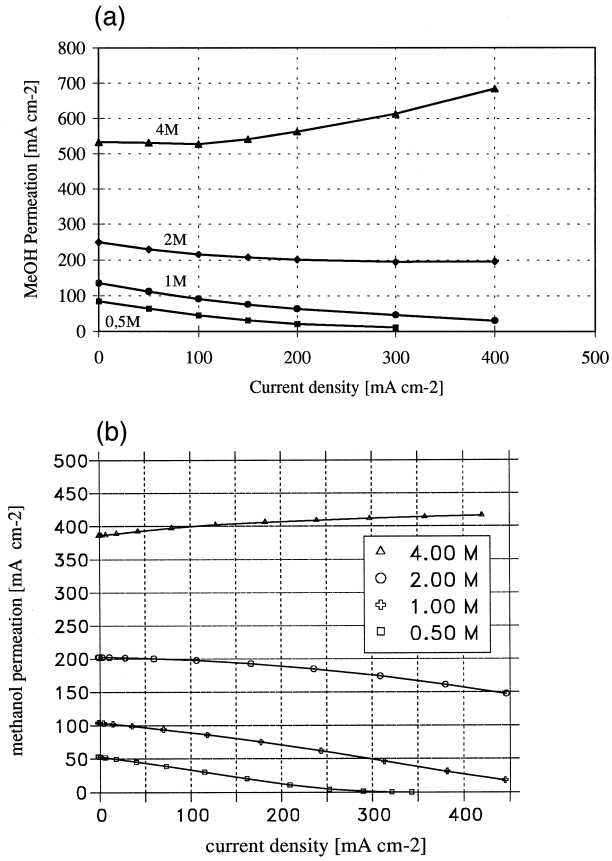

Fig. 5. (a) Influence of methanol concentration on the methanol permeation rate in a DMFC (measurement). (b) Simulation of the influence of the methanol concentration on the methanol permeation rate in a DMFC.

fuel consumption in the anodic catalyst layer, so that less methanol is transmitted to the cathode and the total transport decreases. The electrochemical methanol sink in the anodic catalyst layer now has a restricted acceptance capacity which can be exceeded with increasing concentration, so that the permeation rate at high concentrations increases even further as a consequence of the electro-osmotic drag. This transition is shown in Fig. 5a for a change in concentration from 1 to 4 M. The simulation of the methanol concentration determined experimentally in Fig. 5a on the methanol permeation rate is shown in Fig. 5b.

Even if the simulation shows reasonably good agreement with the experimental data, there is still a discrepancy arising from the influence of the methanol drag. The simulation shows a smaller dependence of the permeation rate on the applied current density than in experiments. This discrepancy is apparently caused by uncertainties in the estimation of the methanol drag factor and its concentration dependence, which has not yet been evaluated and has to be determined experimentally. This work is in progress.

The changes in concentration also have an effect on the overpotential behaviour of the two electrodes. The anodic

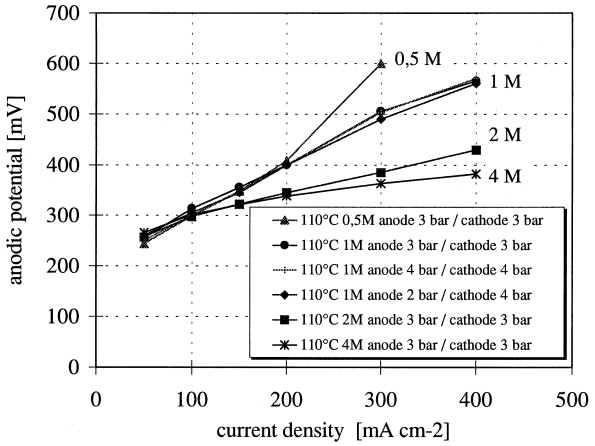

Fig. 6. Influence of the methanol concentration on the anode potential of the DMFC (measurement).

potentials are lowered as the methanol concentration changes from 0.5 to 4 M. With a methanol permeation rate decreasing to zero it may be expected that diffusion overpotentials would arise on the anode side. This was also measured for a methanol concentration of 0.5 M or current densities of 200 mA/cm^2 and above (Fig. 6), where the formation of a concentration overpotential is observed at the lowest methanol concentration of 0.5 M. If the anode potential, and, thus, also the anodic overpotential, decreases with increasing methanol concentration, an increase in cell voltage may be expected with increasing methanol concentration. In this case, however, the methanol permeation rate increases as well (Fig. 5a). If the cathode catalyst is also active towards the anode reaction, formation of a fuel/oxygen mixed potential can be expected on the cathode side. This holds for the platinum cathode catalyst, where a MeOH/O_2 mixed potential is formed at the cathode. This results in a potential shift of the cathode towards negative values, and, thus, in the formation of an additional cathodic overpotential. This is shown in Fig. 7. All these effects can also been explained by simulation.

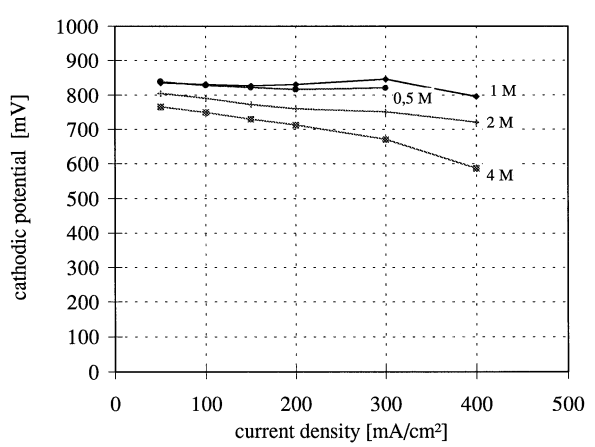

Fig. 7. Influence of the methanol concentration in the anode compartment on the cathode potential of the DMFC (measurement).

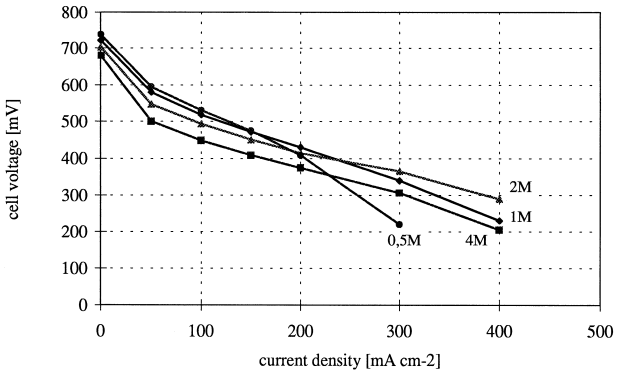

Fig. 8. Current density–voltage curve of a DMFC varying the methanol concentration (measurement).

A comparison of Figs. 6 and 7 shows that with elevated methanol concentrations the losses of cathodic potential caused by increased permeation rates may exceed the potential gains on the anode side so that an overall reduction in total cell voltage involving power losses may result. This is shown in Fig. 8.

An optimum methanol concentration of 2 M is obtained by minimizing the total losses in the given DMFC cell. This can also be confirmed by simulation (Fig. 9).

At lower concentrations, the anodic diffusion overpotentials are too high, whereas the losses in cell voltage caused by the formation of mixed potentials at the cathode side decrease with increasing methanol concentrations so that, overall, an optimum methanol concentration is obtained in the medium concentration range. This may be different for a cell with differently designed electrodes. Fig. 10, for example, shows the possibility for increasing the power density of a DMFC.

This is achieved primarily by compacting the catalyst layer structures to avoid diffusion overpotentials. In practice, compacting can be achieved by the use of unsup-

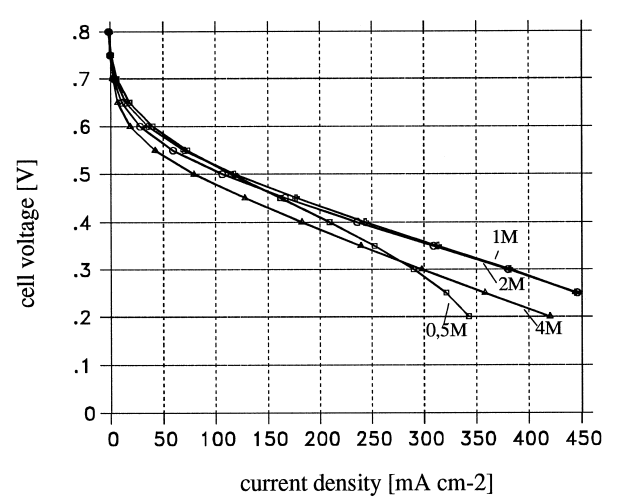

Fig. 9. Simulation of the influence of methanol concentration on the current–voltage curve involving the formation of mixed potentials.

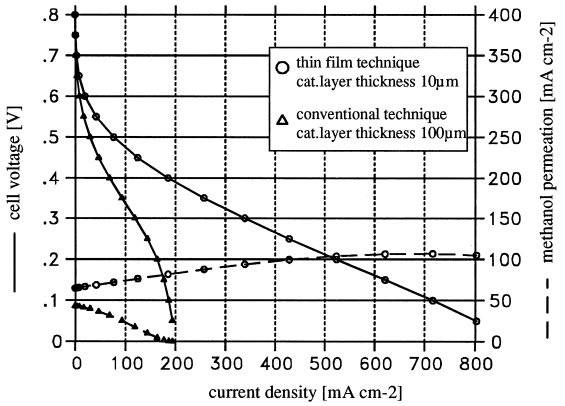

Fig. 10. Simulation of the influence of catalyst layer thickness on the current–voltage curve and the methanol permeation of a DMFC.

ported catalysts. Fig. 10 shows a comparison of the current–voltage curves of two MEAs with the same active area and different layer thicknesses. In addition, methanol permeation is plotted as a function of current density for both MEAs.

The reduced catalyst layer thickness leads to a significant increase in current density under the same operating conditions. Methanol permeation increases with the use of thin film electrodes since the interface between the anodic catalyst layer and the membrane electrolyte still exhibits a relatively high methanol concentration; thus, both the methanol diffusion through the membrane and the electroosmotic drag assume higher values. In this case, lower methanol concentrations will fulfil the optimization conditions.

5. Summary

The electrochemical consumption of methanol in the anodic catalyst layer is a function of concentration and current density. The methanol permeation rate, therefore, depends on the concentration of methanol and on the respective current density. Due to the formation of mixed potentials, caused by concentration-induced methanol permeation, the cathode potential is influenced to such an extent that the augmentation of the potential on the anode side of the cell can be overcompensated by the diminution of the potential in the case of the cathode overpotential.

6. Nomenclature

a	relative humidity
$\mathbf{A}$	coefficient matrix of a system of equations
B_i	transport coefficient of species i in mixture [cm^2/s]
c	concentration [mol/cm^3]
$\underline{c}$	vector of molar concentrations [mol/cm^3]
$\bar{D}$	diffusion coefficient [cm^2/s]
F	Faraday constant = 96487 [A s/mol]
$\mathbf{F}$	transport matrix of the Mean-Transport-Pore-Model [s/cm^2]
$\mathbf{G}$	inverse transport matrix of the Mean-Transport-Pore-Model [cm^2/s]
I	current [A]
i	current density [A/cm^2]
k	proportionality factor
$K_{H,i}$	Henry-constant of species i in mixture [bar cm^3/mol]
N	molar flux [$mol/(cm^2\ s)$]
n_{drag}	drag coefficient (electroosmosis) [mol/mol]
p	pressure [bar]
p_i	partial pressure of species i in mixture [bar]
R	gas constant = 8.31441 [J/(mol K)]
$\langle r \rangle$	mean pore radius [µm]
$\langle r^2 \rangle$	mean square pore radius [µm]
S_{cat}	internal catalyst surface [cm^2/cm^3]
T	absolute temperature [K]
x	direction coordinate [cm]
y_i	mole fraction of species i in the mixture [mol/mol]

Greek symbols

α	transport matrix coefficient [cm^3/mol]
α_a	anodic barrier factor
α_k	cathodic barrier factor
δ	proportionality constant
ε	porosity
φ	potential [V]
γ	Methanol content [$mol_{MeOH}/mol_{SO_3^-}$]
η	dynamic viscosity [Pa s]
λ	stoichiometric air number
σ	conductivity [S cm^{-1}]
ψ	water content [$mol_{H_2O}/mol_{SO_3^-}$]
Ψ	porosity/tortuosity
ζ	transport parameter

Subscripts

0	standard conditions
a	anodic
c	cathodic
d	diffusion
drag	electroosmosis
dry	dry
EC	electrochemical
edge	at the boundary gas channel/MEA
eff	effective
el	electronic
i	species i in mixture
in	at the inlet of the fuel cell
ion	ionic
k	Knudsen
MEA	Membrane Electrode Assembly
mem	membrane electrolyte
out	at the outlet of the fuel cell
p	permeation

ref	reference state
sat	saturated
tot	total

Short cuts

DMFC	Direct methanol fuel cell
FIT	Finite integration technique
MEA	Membrane electrode assembly
MeOH	Methanol
MTPM	Mean transport pore model
PEM	Polymer electrolyte membrane
PTFE	Polytetrafluorethylene

Appendix A. Diffusion and permeation

A.1. Diffusion flux

Stefan–Maxwell:

$$\sum_{j=1}^{n} \frac{y_j N_i^{\mathrm{d}} - y_i N_j^{\mathrm{d}}}{D_{i,j}^{\mathrm{m}}} = -c_{\mathrm{tot}} \frac{\mathrm{d}\, y_i}{\mathrm{d}\, x} \quad i = 1, \ldots, 5$$

$$D_{i,j}^{\mathrm{m}} = \Psi D_{i,j}^{\mathrm{bm}}.$$

Knudsen:

$$N_i^{\mathrm{d}} = -D_i^{\mathrm{k}} c_{\mathrm{tot}} \frac{\mathrm{d}\, y_i}{\mathrm{d}\, x}$$

$$D_i^{\mathrm{k}} = \Psi \langle r \rangle \frac{2}{3} \left(\frac{8RT}{\pi M_i} \right)^{1/2}.$$

Linear combination in the transition range:

$$\frac{N_i^{\mathrm{d}}}{D_i^{\mathrm{k}}} + \sum_{j=1}^{n} \frac{y_j N_i^{\mathrm{d}} - y_i N_j^{\mathrm{d}}}{D_{i,j}^{\mathrm{m}}} = -c_{\mathrm{tot}} \frac{\mathrm{d}\, y_i}{\mathrm{d}\, x}.$$

A.2. Permeation flux

Darcy:

$$N_i^{\mathrm{p}} = -y_i B_i \frac{\mathrm{d}\, c_{\mathrm{tot}}}{\mathrm{d}\, x}$$

$$B_i = D_i^{\mathrm{k}} + \frac{\langle r^2 \rangle \Psi p}{8\eta}.$$

A.3. Total flux

$$N_i = N_i^{\mathrm{d}} + N_i^{\mathrm{p}}.$$

Appendix B. Transport matrix of the MTPM

$$-\frac{\mathrm{d}\underline{c}}{\mathrm{d}\, x} = \mathbf{F}\underline{N}$$

$$f_{i,i} = \frac{1}{D_i^{\mathrm{k}}} + \frac{1}{c_{\mathrm{tot}}} \sum_{\substack{j=1 \\ j \neq i}}^{n} \frac{c_j}{D_{i,j}} + \frac{c_i \alpha_i}{D_i^{\mathrm{k}}} \quad i = 1, \ldots, n$$

$$f_{i,j} = -\frac{c_i}{c_{\mathrm{tot}} D_{i,j}^{\mathrm{m}}} + \frac{c_i \alpha_i}{D_j^{\mathrm{k}}} \quad i \neq j;\ i = 1, \ldots, n;\ j = 1, \ldots, n$$

$$\alpha_i = \frac{\left[1 - \frac{B_i}{D_i^{\mathrm{k}}} + \frac{1}{c_{\mathrm{tot}}} \sum_{\substack{j=1 \\ j \neq i}}^{n} \frac{c_j (B_j - B_i)}{D_{i,j}^{\mathrm{m}}} \right]}{\sum_{j=1}^{n} \frac{c_j B_j}{D_j^{\mathrm{k}}}} \quad 1 = 1, \ldots, n$$

References

[1] T. Biegler, J. Electrochem. Soc. 116 (1969) 1131.
[2] W. Vielstich, Brennstoffzellelemente, Verlag Chemie, Weinheim, 1965.
[3] A.A. Kulikovsky, J. Divisek, A.A. Kornyshev, Modelling the cathode compartment of polymer electrolyte fuel cells: dead and active reaction zones, submitted for publication in J. Electrochemical Soc., June 10, 1999.
[4] H. Dohle, PhD Thesis, RWTH Aachen, submitted.
[5] J. Divisek, J. Mosig, B. Steffen, U. Stimming, F. Lapicque, A. Storck, A.A. Wragg (Eds.), Electrochemical Engineering and Energy, Plenum, New York, 1994, p. 187.
[6] D. Arnost, P. Schneider, Chem. Eng. J. 57 (1995) 91–99.
[7] K. Erhardt, K. Klusacek, P. Schneider, Comput. Chem. Eng. 12 (1988) 1151–1155.
[8] K. Scott, W. Taama, J. Cruickshank, J. Power Sources 65 (1997) 159–171.
[9] J. Wang, R.F. Savinell, Proc. of the Electrochem. Soc., 94-23, p. 326.
[10] T.E. Springer, T.A. Zawodzinski, S. Gottesfeld, J. Electrochem. Soc. 138 (1991) 2334–2341.
[11] X. Ren, W. Henderson, S. Gottesfeld, J. Electrochem. Soc. 144 (1997) 267–270.
[12] M.V. Verbrugge, J. Electrochem. Soc. 136 (1989) 417–423.